

Copyright © 1982, by the author(s).
All rights reserved.

Permission to make digital or hard copies of all or part of this work for personal or classroom use is granted without fee provided that copies are not made or distributed for profit or commercial advantage and that copies bear this notice and the full citation on the first page. To copy otherwise, to republish, to post on servers or to redistribute to lists, requires prior specific permission.

NONADIABATIC SCATTERING AND PARTICLE FLOW
IN MULTIPLE MIRRORS

by

K.J. Doniger and M.A. Lieberman

Memorandum No. UCB/ERL M82/47

20 May 1982

ELECTRONICS RESEARCH LABORATORY

College of Engineering
University of California, Berkeley
94720

NONADIABATIC SCATTERING AND PARTICLE FLOW
IN MULTIPLE MIRRORS

K.J. Doniger and M.A. Lieberman
Department of Electrical Engineering and Computer Sciences
and the Electronics Research Laboratory
University of California, Berkeley, California 94720

ABSTRACT

Two types of longitudinally asymmetric multiple mirrors are explored. One has sudden magnetic field jumps and the other has smooth jumps in the field. The changes in magnetic moment and gyrophase are derived for rightward moving and leftward moving particles for each field type. In the "smooth" case, there is no difference between right and left. A difference is found in the "sudden" case. Mapping equations are developed and trapping probabilities are estimated for this case. If there are no interparticle collisions, then there is no net flow of particles in either direction. If interparticle collisions isotropize the distribution to any extent, a net flow is found.

This research is sponsored by the National Science Foundation Grant No. ECS-8104561 and the U.S. Office of Naval Research Contract No. N00014-79-C-0674.

INTRODUCTION

In a recent paper¹, Post and Li showed that if the detrapping probability in a mirror cell could be made directionally dependent, particle confinement time in a multiple mirror would be increased. The authors did not, however, propose a mechanism to achieve this asymmetry. The purpose of this report is to investigate nonadiabatic scattering of the magnetic moment, μ , in a multiple mirror composed of longitudinally asymmetric cells as a possible mechanism.

Two models are discussed in this paper. The first, in section I, is the "sawtooth field" (see Fig. 1). It is physically unrealistic but mathematically simple and may be considered as the limit of the case where the magnetic field changes quickly compared to the gyrophase in the nonadiabatic region. The second, in section II, consists of a generalized paraxial field where the gyrophase in the nonadiabatic region varies more rapidly than the field itself. For purposes of calculation, a field consisting of back-to-back hyperbolic tangents was chosen (see Fig. 2).

In both models, the field is symmetric about the magnetic axis, so the canonical angular momentum is constant. Because a static magnetic field can do no work, energy is conserved as well.

SECTION I

Consider a system where the magnetic field is as shown in Fig. 1. The slope of the ramp between discontinuities is exaggerated. In fact, B_z varies slowly enough that B_r can be neglected everywhere except at the jumps where the change in B_z is instantaneous. Particle orbits are approximately helical and the magnetic vector potential may be written

$$\underline{A}(r,z) = \frac{1}{2} \Omega r \hat{\theta}$$

where $\Omega = eB_z/m$. In cartesian coordinates this is

$$A_x = -\frac{1}{2} \Omega y$$

$$A_y = \frac{1}{2} \Omega x.$$

Two systems of canonical coordinates will be used. Cartesian (or "C" for short) coordinates consist of x, P_x, y, P_y, z, P_z where P is the canonical momentum.

$$P_x = V_x - \frac{1}{2} \Omega y$$

$$P_y = V_y + \frac{1}{2} \Omega x$$

$$P_z = V_z$$

Note that charge and mass have been set equal to 1. Guiding center (or "G" for short) coordinates consist of $\phi, \mu, \theta_g, \psi, z, P_z$ (see Fig. 3) where

$$\mu = -\frac{1}{2\Omega} (V_x^2 + V_y^2)$$

is the magnetic moment,

$$\phi = \arctan (V_x / -V_y)$$

is the gyrophase,

$$\psi = \frac{1}{2} \Omega (X_g^2 + Y_g^2)$$

is the radial flux coordinate (X_g and Y_g are the x and y coordinates of the guiding center), and

$$\theta_g = \arctan (Y_g / X_g).$$

The axial distance z and its conjugate momentum P_z are the same as in Cartesian coordinates. The angles ϕ and θ_g are both referenced to the x axis. Note that μ is defined negative. This makes the "G" coordinates canonical.

As mentioned in the introduction, there are two constants of the motion, total kinetic energy and canonical angular momentum, P_θ . These two constants are used to reduce the problem from 3 degrees of freedom to 1 degree of freedom. To do this, we must first generate jump conditions.

Consider a particle moving an infinitesimal distance in z , across a magnetic discontinuity. On either side of the jump, the field is well defined and is in the \hat{z} direction, at the discontinuity itself, the field value is undefined, but its direction is known to be radial. In an infinitesimal distance, the particle location doesn't change. Therefore, x and y are constant across a jump. The fact that the canonical radial momentum, $P_r = V_r m$, together with the Lorentz force law

$$\dot{\underline{V}} = \underline{V} \times \underline{\Omega} ,$$

shows that P_r is constant across a jump. Since P_θ is always constant, P_x and P_y are constant across a jump. Thus, we see that all perpendicular cartesian coordinates are constant across a discontinuity.

As the particle traverses the slowly varying region (the ramp), its motion is given by the drift equations. Since we are ignoring B_r in this region, μ , θ_g and ψ are constant. The gyrophase, ϕ , varies in a simple way. If B_r in this region was included in the analysis, there would be a small, azimuthal, guiding center drift.

The transformations between "C" and "G" variables are

$$\phi = \arctan \left[\frac{P_x + \frac{1}{2} \Omega y}{-P_y + \frac{1}{2} \Omega x} \right]$$

$$\mu = -\frac{1}{2\Omega} \left[(P_x + \frac{1}{2} \Omega y)^2 + (P_y - \frac{1}{2} \Omega x)^2 \right]$$

$$\theta_g = \arctan \left[\frac{-P_x + \frac{1}{2} \Omega y}{P_y + \frac{1}{2} \Omega x} \right]$$

$$\psi = \frac{1}{2\Omega} \left[(P_x - \frac{1}{2} \Omega y)^2 + (P_y + \frac{1}{2} \Omega x)^2 \right]$$

$$x = \sqrt{\frac{2}{\Omega}} \left[\sqrt{-\mu} \cos \phi + \sqrt{\psi} \cos \theta_g \right]$$

$$P_x = \sqrt{\frac{\Omega}{2}} \left[\sqrt{-\mu} \sin \phi - \sqrt{\psi} \sin \theta_g \right]$$

$$y = \sqrt{\frac{2}{\Omega}} \left[\sqrt{-\mu} \sin \phi + \sqrt{\psi} \sin \theta_g \right]$$

$$P_y = \sqrt{\frac{\Omega}{2}} \left[-\sqrt{-\mu} \cos \phi + \sqrt{\psi} \cos \theta_g \right].$$

In addition,

$$P_\theta = \psi + \mu.$$

We normalize these transformations by setting the total velocity V , and Ω_0 (eB₀/m) equal to 1. Now, $1 \leq \Omega \leq R$ where R is the mirror ratio and the magnetic moment, μ ranges from 0 to $-1/2$.

A particle will reflect from a jump if conservation of energy cannot be satisfied through the jump. To see how this works, imagine a particle about to cross a jump. The particle has well defined "G" and "C" coordinates μ , x , y , P_x , P_y . The field strength is Ω . After traveling an infinitesimal distance (across the jump), x , y , P_x , and P_y are unchanged but the field strength is now $\bar{\Omega}$. Using the transformation equations, we get a new magnetic moment, $\bar{\mu}$. If $2\bar{\Omega}|\bar{\mu}| > 1$, then the perpendicular energy is greater than the total energy. This is impossible, so the particle must reflect. Since μ is a function of the perpendicular "C" coordinates and field strength, $\bar{\mu} = \mu$ after a reflection. This

applies to the other perpendicular "G" coordinates as well ($\bar{\psi}=\psi$, $\bar{\phi}=\phi$, $\bar{\theta}_g = \theta_g$), but only $\bar{\mu}$ has a role in determining reflection.

Note that z and P_z have all but disappeared from these calculations. We will drop them from the "C" and "G" coordinates.

We now develop a mapping from surface-of-section to surface-of-section. These surfaces are located an infinitesimal distance to the left of each jump.

We first consider the case of a particle moving through a surface-of-section in the positive direction (to the right). If the particle passes (see Fig. 4):

- 1) Use the "C" coordinates before the jump at $\Omega = 1$ to get the " \bar{G} " coordinates after the jump at $\Omega = R$. (Point 1 to Point 2)

- 2) The " \bar{G} " coordinates, $\bar{\mu}$, $\bar{\psi}$ and $\bar{\theta}_g$ remain constant to the next surface-of-section. $\bar{\phi}$ changes according to a winding function which will be given explicitly later. (Point 2 to Point 3)

- 3) Use the " \bar{G} " coordinates at the surface-of-section (Point 3) to get " \bar{C} ."

If the particle reflects, all "C" and "G" coordinates remain constant.

Suppose the particle moves through the surface-of-section in the negative direction (to the left). If the particle passes (see Fig. 4):

- 1) μ , ψ and θ_g remain constant on the ramp. ϕ changes according to a winding function. Use these "G" coordinates to get the "C" coordinates at $\Omega = R$ (Point 1 to Point 4).

- 2) After the jump, use "C" to get " \bar{G} " at $\Omega = 1$. (Point 4 to Point 5)

If the particle reflects, then μ , ψ and θ_g remain constant. ϕ changes according to a winding function. All "C" coordinates change.

In the actual mapping equations, the move from one surface-of-section to the next will be handled in one step and only guiding center coordinates will be used.

We will now make explicit the winding function mentioned earlier.

$$\begin{aligned}\bar{\phi} &= \phi - \int_0^t \Omega(\tau) d\tau \\ &= \phi - \int_0^z \frac{\Omega(\zeta)}{V_z(\zeta)} d\zeta \\ &= \phi - I\end{aligned}$$

If we take $z=0$ at the surface-of-section,

$$\begin{aligned}\Omega(z) &= 1 - \frac{R-1}{d} z \\ &= 1 - \alpha z\end{aligned}$$

where d is the (dimensionless) cell length and $\alpha \ll 1$ to insure a gradual slope. Note that $z < 0$.

$$V_z(z) = \sqrt{1 + 2\Omega(z)\mu}$$

If the particle travels a full cell length, the winding function is

$$I_1(\mu) = \frac{1}{3\alpha\mu} \left(1 - \frac{1}{\mu}\right) \sqrt{1 + 2\mu} - \frac{1}{3\alpha\mu} \left(R - \frac{1}{\mu}\right) \sqrt{1 + 2\mu R}.$$

If the particle is moving up a ramp and the magnitude of μ is large enough, it will reflect before it reaches the jump at the top of the ramp. In this case, the winding function is

$$I_2(\mu) = \frac{2}{3\alpha\mu} \left(1 - \frac{1}{\mu}\right) \sqrt{1 + 2\mu}.$$

The mapping equations will now be presented case by case as in Fig. 5. The mapping equations have been shown numerically to be area preserving and give explicit expressions for the new (barred) variables in terms of the old (unbarred) ones.

If the particle moves to the left and passes through the jump, the equations are

$$\bar{\mu} = \frac{1}{4R} \left[(R+1)^2 \mu - (R-1)^2 \psi + 2(R^2-1) \sqrt{-\mu\psi} \cos(\theta_g - \phi + I_1) \right]$$

$$\bar{\psi} = \frac{1}{4R} \left[(R+1)^2 \psi - (R-1)^2 \mu - 2(R^2-1) \sqrt{-\mu\psi} \cos(\theta_g - \phi + I_1) \right]$$

$$\bar{\phi} = \arctan \left[\frac{(R+1) \sqrt{-\mu} \sin(\phi - I_1) - (R-1) \sqrt{\psi} \sin \theta_g}{(R+1) \sqrt{-\mu} \cos(\phi - I_1) - (R-1) \sqrt{\psi} \cos \theta_g} \right]$$

$$\bar{\theta}_g = \arctan \left[\frac{(R+1) \sqrt{\psi} \sin \theta_g - (R-1) \sqrt{-\mu} \sin(\phi - I_1)}{(R+1) \sqrt{\psi} \cos \theta_g - (R-1) \sqrt{-\mu} \cos(\phi - I_1)} \right]$$

where $I_1 = I_1(\mu)$. This is case 1 in Fig. 5.

If the particle moves to the left and reflects off the jump, μ , ψ , and θ_g are unchanged.

$$\bar{\phi} = \phi - 2I_1(\mu)$$

This is case 2.

If the particle moves to the left and reflects before reaching the jump, μ , ψ and θ_g are unchanged.

$$\bar{\phi} = \phi - I_2(\mu)$$

This is case 3.

If the particle moves to the right and reflects, all variables are unchanged. This is case 4.

If the particle moves to the right and passes through the jump, the equations are

$$\bar{\mu} = \frac{1}{4R} \left[(R+1)^2 \mu - (R-1)^2 \psi - 2(R^2-1) \sqrt{-\mu\psi} \cos(\theta_g - \phi) \right]$$

$$\bar{\psi} = \frac{1}{4R} \left[(R+1)^2 \bar{\mu} - (R-1)^2 \psi + 2(R^2-1) \sqrt{-\mu\psi} \cos(\theta_g - \phi) \right]$$

$$\bar{\phi} = \arctan \left[\frac{(R+1) \sqrt{-\mu} \sin(\phi - \bar{I}_1) + (R-1) \sqrt{\psi} \sin(\theta_g - \bar{I}_1)}{(R+1) \sqrt{\mu} \cos(\phi - \bar{I}_1) + (R-1) \sqrt{\psi} \cos(\theta_g - \bar{I}_1)} \right]$$

$$\bar{\theta}_g = \arctan \left[\frac{(R+1) \sqrt{\psi} \sin \theta_g + (R-1) \sqrt{-\mu} \sin \phi}{(R+1) \sqrt{\psi} \cos \theta_g + (R-1) \sqrt{-\mu} \cos \phi} \right]$$

where $\bar{I}_1 = I_1(\bar{\mu})$. This is case 5.

Earlier in this section, a degree of freedom (z, P_z) was removed from the problem by using the conservation of energy. The second constant of the motion, P_θ , will now be used to eliminate ψ and θ_g reducing the problem to a non-autonomous system in one degree of freedom. We set

$$\psi = P_\theta - \mu,$$

and redefine ϕ as shown in Fig. 6. In addition we multiply μ by -2.

The magnetic moment will now range from 0 to 1. The mapping equations are then as follows:

Case 1)

$$\bar{\mu} = \mu + \frac{1}{2R} \left[(R-1)^2 (\mu + P_\theta) - (R^2-1) \sqrt{\mu(\mu+2P_\theta)} \cos(\phi - I_1) \right]$$

$$\bar{\phi} = \arctan \left[\frac{2R \sqrt{\mu(\mu+2P_\theta)} \sin(\phi - I_1)}{(R^2+1) \sqrt{\mu(\mu+2P_\theta)} \cos(\phi - I_1) - (R^2+1)(\mu+P_\theta)} \right]$$

Case 2) Trapped because $\bar{\mu} > 1$

$$\bar{\mu} = \mu$$

$$\bar{\phi} = \phi - 2I_1$$

Case 3) Trapped because $\mu > 1/R$

$$\bar{\mu} = \mu$$

$$\bar{\phi} = \phi - I_2$$

Case 4) Trapped because $\bar{\mu} > 1/R$

$$\bar{\mu} = \mu$$

$$\bar{\phi} = \phi$$

Case 5)

$$\bar{\mu} = \mu + \frac{1}{2R} \left[(R-1)^2 (\mu + P_\theta) + (R^2-1) \sqrt{\mu(\mu+2P_\theta)} \cos \phi \right]$$

$$\bar{\phi} = \arctan \left[\frac{2R \sqrt{\mu(\mu+2P_\theta)} \sin \phi}{(R^2+1) \sqrt{\mu(\mu+2P_\theta)} \cos \phi + (R^2-1)(\mu+P_\theta)} \right] - \bar{I}_1$$

where

$$I_1 = -\frac{2}{3\alpha\mu} \left(1 + \frac{2}{\mu}\right) \sqrt{1-\mu} + \frac{2}{3\alpha\mu} \left(R + \frac{2}{\mu}\right) \sqrt{1-R\mu}$$

$$\bar{I}_1 = I_1(\bar{\mu})$$

$$I_2 = -\frac{4}{3\alpha\mu} \left(1 + \frac{2}{\mu}\right) \sqrt{1-\mu} .$$

Note that there are differences between cases 1 and 5.

The mapping equations were numerically integrated. Some typical μ - ϕ phase planes are shown in Figs. 7-10. Each figure consists of two planes; one for particles crossing the surface-of-section leftward ($V_z < 0$), the other for particles crossing rightward ($V_z > 0$). Each phase plane is then split into passing and trapped orbits. (There are 4 plots in each figure.) One can see that the two complete phase planes in each figure are mirror images of each other. It is when each phase plane is

split in the aforementioned way that the difference emerges.

In figures 7-10, the mirror ratio is 1.33 and the normalized cell length is 100 ($\alpha = .0033$). P_θ is varied over the four figures. Since

$$P_\theta = \frac{1}{2} (X_g^2 + Y_g^2) - \frac{1}{2} \mu$$

and the range of μ is limited ($0 \leq \mu \leq 1$), increasing P_θ indicates an increasing guiding center radius.

The major question to be answered is whether the directional difference shown in figures 7-10 does in fact result in different trapping probabilities in the two directions.

To estimate the trapping probability, note that in the regime of interest ($\alpha \ll 1$), particles make many gyro-orbits between surfaces-of-section. The gyrophase may be regarded as random and, therefore, uniformly distributed. For $\alpha \ll 1$, the phase plane is predominantly stochastic. We will assume that the non-stochastic area of the phase plane is unimportant.

If there are no particle-particle interactions, the distribution in μ is uniform over the entire phase plane. This has been verified numerically. The trapping probability is then the ratio of "trapped" phase space area to total phase space area.

Note that a uniform distribution in μ does not correspond to a uniform distribution of pitch angles (an isotropic distribution). The latter would be a consequence of strong interparticle collisions between jumps which isotropize the distribution of pitch angles.

We now estimate the trapping probabilities for $V_z > 0$ and $V_z < 0$.

For V_z positive, we have $\bar{\mu} > 1/R$ as necessary and sufficient for trapping. Substituting for $\bar{\mu}$ in case 1, we get an equation of the form

$$C + D \cos \phi > 0$$

for trapping, where C and D are functions of μ , P_θ , and R. D is always non-negative. If $|C| > D$, then the particle is always trapped or never trapped depending on the sign of C. If $|C| < D$, then there are critical phases given by

$$\phi_c = \pm \arccos(-C/D)$$

That mark the boundaries between passing and trapped orbits. For a given R, P_θ , and μ , the fraction of the phases which are trapped is $\phi_c(\mu; P_\theta, R)/\pi$. For these two cases, denote the fraction of trapped phases as $F_+(\mu; P_\theta, R)$.

A similar calculation gives $F_-(\mu; P_\theta, R)$ for $V_z < 0$.

The relationship between magnetic moment and δ_0 , the pitch angle at $\Omega = 1$, is

$$\mu = \sin^2 \delta_0.$$

To get the total trapping probability for a given P_θ and R, we integrate F_\pm over μ . If there are no interparticle effects, the μ distribution is uniform. The total trapping probability is given by

$$P_\pm = \int_0^1 F_\pm(\mu; P_\theta, R) d\mu.$$

If collisions isotropize the distribution between jumps,

$$P_\pm = \int_0^1 F_\pm(\mu; P_\theta, R) \frac{d\mu}{2\sqrt{1-\mu}}.$$

By isotropic, we mean a constant number of particles per unit solid angle in velocity space.

The results of these calculations are shown in figures 11-14. F_+ and F_- are numerically evaluated and graphed. P_+ and P_- for the collisionless case are given just beneath the initial conditions. Note that the

two values are the same for all four examples: .248 for $P_\theta = 0$, .327 for $P_\theta = 2$, .511 for $P_\theta = 10$, and .886 for $P_\theta = 50$. In the collisionless case, there is no difference between the two directions.

For the collisional case, the results of Figs. 11-14 are summarized in the following table.

P_θ	P_+	P_-
0.0	.449	.488
2.0	.463	.555
10.0	.568	.680
50.0	.842	.907

Note that $P_- > P_+$. In a collisional system, particles will be more likely to escape out the right end of each cell.

As an aside, note that as P_θ increases, so does the total trapping probability. In the extreme case where

$$P_\theta \geq \frac{4(R+1)}{(R-1)^2}$$

both P_+ and P_- are equal to 1 (regardless of the distribution), and no particles escape.

SECTION II

In this section, the more common situation where the field changes slightly during a gyroperiod, will be explored. A calculation of the type in section I cannot be done. A perturbative approach must be used instead. The calculation has been done and will be repeated in this section, following most closely the treatment in References 2 and 3. We have developed a simple formula for changes in magnetic moment in a

static, axisymmetric, vacuum field.

Define a normalized magnetic moment

$$\mu = \frac{B_0 V_{\perp}^2}{B V^2} \quad (2.1)$$

where B_0 is the minimum value of the field, and V is the total velocity (a constant). μ ranges from 0 to 1. Using the single particle equation of motion we get

$$\dot{\mu} = \frac{2B_0}{V^2} \left[\frac{V_{\perp}}{B} \frac{dV_{\perp}}{dt} - \frac{V_{\perp}^2}{2B} \frac{dB}{dt} \right],$$

and assuming no currents in the plasma,

$$\dot{\mu} = -\frac{2B_0}{V^2} \left[\frac{1}{B^2} (V_{\parallel}^2 + \frac{1}{2} V_{\perp}^2) (\underline{V}_{\perp} \cdot \nabla B) + \frac{V_{\parallel} V_{\perp}^2}{2B^2} \nabla_{\parallel} B + \frac{V_{\parallel}}{B^2} \underline{V}_{\perp} \cdot (\underline{V}_{\perp} \cdot \nabla) \underline{B} \right]$$

Let $\underline{V}_{\perp} = V_{\perp} \cos \phi \hat{e}_1 - V_{\perp} \sin \phi \hat{e}_2$ where ϕ is the gyrophase and \hat{e}_1 and \hat{e}_2 are right-handed orthonormal vectors perpendicular to the field. Let

$$(\underline{V}_{\perp} \cdot \nabla) B = V_{\perp} B \rho_{\perp} \cos \phi$$

where ρ_{\perp} is the perpendicular field curvature. Then

$$\begin{aligned} \dot{\mu} = & -\sqrt{\frac{B_0}{B}} \mu \left(2 - \frac{B}{B_0} \mu \right) V \rho_{\perp} \cos \phi \\ & + \text{terms involving } \cos(2\phi) \text{ and } \sin(2\phi) \end{aligned} \quad (2.2)$$

The equation for the gyrophase is

$$\dot{\phi} = -\Omega \quad (2.3)$$

to lowest order. Defining L as a magnetic scale length and $\Omega_0 = eB_0/m$, let

$$\epsilon = V/L\Omega_0. \quad (2.4)$$

In the limit where $\epsilon \ll 1$, the terms involving $\cos(2\phi)$ and $\sin(2\phi)$ will

be exponentially small and can be dropped. Solving (2.2), we get

$$\frac{\Delta\mu}{\mu} = - \int \sqrt{\frac{B_0}{\mu B}} \frac{(2 - \mu B/B_0)}{\sqrt{1 - \mu B/B_0}} \rho_{\perp} \cos \phi \, ds \quad (2.5)$$

where s is the arc length along a field line. We have assumed that the changes in μ are small enough that μ can be considered constant under the integral. This restricts the validity of the analysis to magnetic moments greater than some minimum value. We extend the limits of the integration in (2.5) to $\pm\infty$. This will allow us to obtain the integral by asymptotic means, but it limits the analysis to fields whose non-adiabatic portions are well separated. In other words, one jump in μ must be finished before the next can begin. Since the jumps are of short duration (on the order of a gyroperiod), this is rarely a problem.

We change variables in (2.5) from s to ϕ and go into the complex ϕ plane to get

$$ds = - \frac{V}{\Omega} \sqrt{1 - \mu B/B_0} \, d\phi$$

and

$$\frac{\Delta\mu}{\mu} = \text{Re} \int_C \sqrt{\frac{B_0}{\mu B}} \left(2 - \frac{\mu B}{B_0}\right) \frac{V\rho_{\perp}}{\Omega} e^{i\phi} \, d\phi \quad (2.6)$$

Because the gyromotion is much faster than the magnetic field variation as seen by the particle guiding center, the integral will be dominated by the stationary phase points of ϕ . From (2.3) these points are seen to be the complex zeros of B . Since the important contributions to (2.6) come from places where $B \approx 0$, (2.6) can be simplified to

$$\frac{\Delta\mu}{\mu} = \frac{2\varepsilon}{\sqrt{\mu}} \text{Re} \int_C \left(\frac{B_0}{B}\right)^{3/2} \rho_{\perp L} e^{i\phi} \, d\phi \quad (2.7)$$

where ε is defined in (2.4). The rapid phase assumption puts an energy

related lower bound on μ . A particle must execute many gyroorbits while traversing a magnetic scale length. If a particle has too much parallel energy, this condition will not be satisfied.

Solving Eq. (2.3) we get

$$\phi = \phi_0 - \int_{s_0}^s \frac{\Omega ds}{v \sqrt{1-\mu B/B_0}} \quad (2.8)$$

We will now specialize to axisymmetric fields with no internal currents. Such fields can be expanded paraxially.

$$\frac{B_z}{B_0} = f(z/L) - \frac{1}{4} f''(z/L) \frac{r^2}{L^2} + \dots \quad (2.9a)$$

$$\frac{B_r}{B_0} = -\frac{1}{2} f'(z/L) \frac{r}{L} + \frac{1}{16} f'''(z/L) \frac{r^3}{L^3} - \dots \quad (2.9b)$$

where a prime denotes differentiation with respect to the argument, and $f(z/L)$ is the on-axis field. This expansion is good for $r \ll L$, and is also known as the long, thin approximation. We define a stream function, ψ , such that

$$\frac{B_z}{B_0} = \frac{L^2}{r} \frac{\partial \psi}{\partial r} \quad (2.10a)$$

$$\frac{B_r}{B_0} = -\frac{L^2}{r} \frac{\partial \psi}{\partial z} \quad (2.10b)$$

ψ is the radial flux coordinate. Choosing ψ specifies a field line (up to an arbitrary angle). If we assume that a particle guiding center stays on a given flux surface, then ψ is a constant. This is not strictly true. As in Section 1, P_θ , which is a function of μ and ψ , is the true constant of the motion. As μ varies, so will ψ . However, if μ doesn't change much (as in the present case where $\Delta\mu/\mu \ll 1$), keeping ψ constant is a good approximation, and a great simplification. Solving Eq.'s (2.10) for ψ , we get

$$\psi = \frac{1}{2} f(z/L) \frac{r^2}{L^2} + \frac{1}{16} f''(z/L) \frac{r^4}{L^4} + \dots \ll 1$$

Note that if $f(z/L) = \text{constant}$, ψ reduces to that of section 1. Inverting the series,

$$\frac{r^2}{L^2} = \frac{2}{f} \psi + \frac{f''}{2f^3} \psi + \dots$$

We substitute this into the field Eqs. (2.9) to get

$$\frac{B_z}{B_0} = f - \frac{f''}{2f} \psi + \dots \quad (2.11a)$$

$$\frac{B_r}{B_0} = -f' \sqrt{\frac{\psi}{2f}} + \dots \quad (2.11b)$$

Evaluating ρ_{\perp} to lowest order in ψ we obtain

$$\begin{aligned} \rho_{\perp} &= \frac{\frac{\partial}{\partial r} \left(\frac{B_z}{B_r} \right)}{\left[1 + (B_z/B_r)^2 \right]^{3/2}} \\ &= -\frac{1}{4L} \sqrt{2\psi f} f'^2 \left(\frac{B_0}{B} \right)^3. \end{aligned} \quad (2.12)$$

Substituting (2.12) into (2.7), we have

$$\frac{\Delta \mu}{\mu} = -\epsilon \sqrt{\frac{\psi}{2\mu}} \operatorname{Re} \int_C \left(\frac{B_0}{B} \right)^{9/2} f^{1/2} f'^2 e^{i\phi} d\phi \quad (2.13)$$

To solve (2.13), the complex zeros of B , \hat{z}_n , must be found. At $z = \hat{z}_n$,

$$f^2 + \left[\frac{f'^2}{2f} - f'' \right] \psi = 0$$

For small ψ , this is a triplet of roots clustered about each root of $f(z/L)$. We let z_n be the roots of f , set $B \sim B_0 f$, and expand B about z_n to obtain

$$\frac{B}{B_0} = f'(z_n/L) (z - z_n)/L \quad (2.14)$$

Then (2.13) becomes

$$\frac{\Delta\mu}{\mu} = -3 \epsilon \sqrt{\frac{\psi}{2\mu}} \sum_n \operatorname{Re} \left[\frac{1}{f'^2(z_n/L)} \int_c \left(\frac{z-z_n}{L} \right)^{-4} e^{i\phi} d\phi \right]. \quad (2.15)$$

Each element in the sum is a triplet and this accounts for the factor of 3 in (2.15). Using Eqs. (2.8) and (2.14), we relate phase, ϕ , to z at z_n .

$$\begin{aligned} \phi - \phi_n &= -\frac{1}{\epsilon} \int_{z_n}^z \frac{B/B_0}{\sqrt{1-\mu B/B_0}} \frac{dz}{L} \\ &\approx -\frac{f'(z_n/L)}{\epsilon} \int_{z_n}^z \frac{z-z_n}{L} dz. \end{aligned}$$

From this, we conclude

$$\left(\frac{z-z_n}{L} \right)^{-4} = \frac{f'^2(z_n/L)}{4^2} (\phi - \phi_n)^{-2}. \quad (2.16)$$

Let $W = i(\phi - \phi_n)$ and substitute (2.16) into (2.15). In the complex W plane, the contour of integration is the Hankel contour (Fig. 15).

Solving (2.15) we obtain

$$\frac{\Delta\mu}{\mu} = \frac{3\pi}{2\epsilon} \sqrt{\frac{\psi}{2\mu}} \sum_n \exp \left[-\operatorname{Im}(\phi_n - \phi_0) \right] \cos \left[\phi_0 + \operatorname{Re}(\phi_n - \phi_0) \right] \quad (2.17)$$

where

$$\phi_n - \phi_0 \approx -\frac{1}{\epsilon} \int_{z_0}^{z_n} \frac{f}{\sqrt{1-\mu f}} d\left(\frac{z}{L}\right) \quad (2.18)$$

$f(z_n/L) = 0$, and z_0 is some reference point.

As an example, consider the field in Fig. 2, which consists of two hyperbolic tangents with different scale lengths placed back to back. Since the magnitude of the change in magnetic moment goes as $\exp(-\text{scale})$, we consider motion on the "long" tanh to be adiabatic. The on-axis field of the "short" tanh is

$$f(z/L) = \frac{1}{2} (R+1) + \frac{1}{2} (R-1) \tanh(z/L) \quad (2.19)$$

where R is the mirror ratio (see Fig. 16). The complex roots of f are

$$z_n = -\frac{1}{2} \ln R + i \left(n - \frac{1}{2}\right) \pi \quad n = 1, 2, 3, \dots$$

The imaginary parts of these roots are well separated, so the root nearest the real axis, z_1 , dominates the sum in (2.17). The jump in μ will take place around the point $\text{Re}(z_1)$ which is marked with an "x" in Fig. 16. From (2.18)

$$\phi_1 - \phi_0 = \frac{i\pi}{2\varepsilon\sqrt{1-\mu}} + \text{Re}(\phi_1 - \phi_0).$$

$\text{Re}(\phi_1 - \phi_0)$ is a complicated function of μ and R . From (2.17),

$$\frac{\Delta\mu}{\mu} = \frac{3\pi}{2\varepsilon} \sqrt{\frac{\psi}{2\mu}} \exp \left[-\frac{\pi}{2\varepsilon\sqrt{1-\mu}} \right] \cos \left[\phi_0 + \text{Re}(\phi_1 - \phi_0) \right] \quad (2.20)$$

Equation (2.20) has been verified by direct integration of the equations of motion using the particle orbit code, TIBRO, and is in excellent agreement with the TIBRO results for $\psi \leq .125$.

Note that neither (2.17) nor (2.18) have any directional dependence. So, to first order, the sign of V_z makes no difference, there is no loss cone asymmetry. Since we are limited in this case to jumps in magnetic moment less than 10%, second order effects will be too small to be of any importance.

CONCLUSION

We have shown that nonadiabatic scattering in static, axisymmetric magnetic fields will produce a loss cone asymmetry under the following conditions:

- 1) The field varies quickly compared to the gyrophase.
- 2) The plasma is collisional.

This loss cone asymmetry produces a net flow of particles. All of the

preceeding calculations are for single particles only. Collective effects have been ignored.

ACKNOWLEDGEMENTS

This research supported by National Science Foundation Grant ECS-8104561 and the U.S. Office of Naval Research Contract No. N00014-79-C-0674.

REFERENCES

1. R.F. Post and X.Z. Li, Nuclear Fusion, 21, 135 (1981).
2. R.J. Hastie and J.E. Howard, Private communication.
3. R.H. Cohen, G. Rowlands and J.H. Foote, Phys. Fluids, 21, 627 (1978).

FIGURE CAPTIONS

Fig. 1. Sawtooth Field. The dotted lines are surfaces-of-section. The vertical scale of the upper plot is exaggerated. The arrows on the plot are Dirac Delta functions.

Fig. 2. On-axis field for the "smooth" case.

Fig. 3. Relationship between Cartesian and Guiding Center Coordinates.

$$\chi = \frac{1}{2}\Omega R_g^2, \quad \mu = -\frac{1}{2}\Omega r_L^2.$$

Fig. 4. To generate the map for passing particles, we start at Point 1 and finish at Point 3 or Point 5.

Fig. 5. The 5 different types of orbit. The dotted lines are surfaces-of-section. The crosses indicate where the orbits encounter field discontinuities.

Fig. 6. The redefinition of ϕ .

Fig. 7-10. Plots of the μ - ϕ phase plane. Mirror ratio = 1.33, $\alpha = .0033$, $P\theta = 0.0$ in Fig. 7, 2.0 in Fig. 8, 10.0 in Fig. 9, and 50.0 in Fig. 10.

Fig. 11-14 Trapping possibilities.

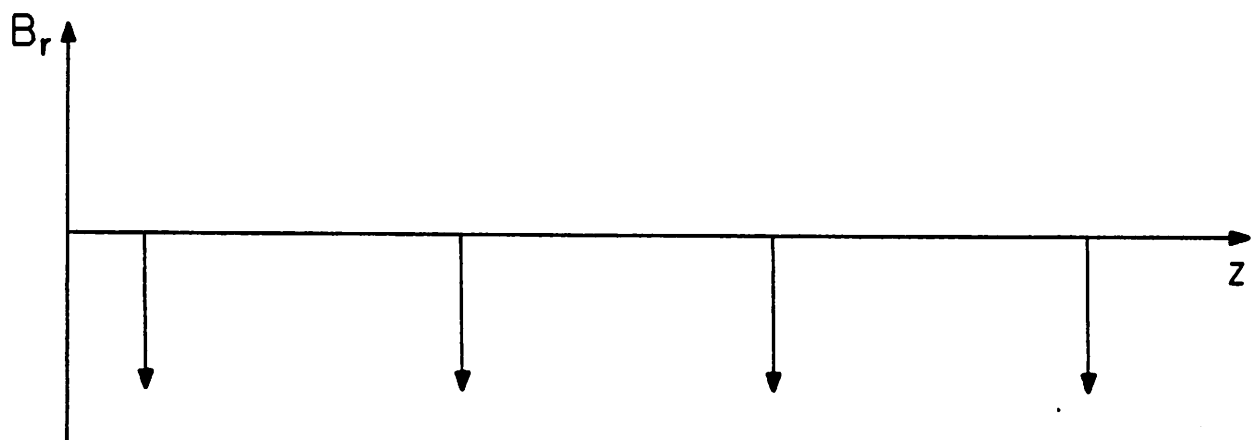
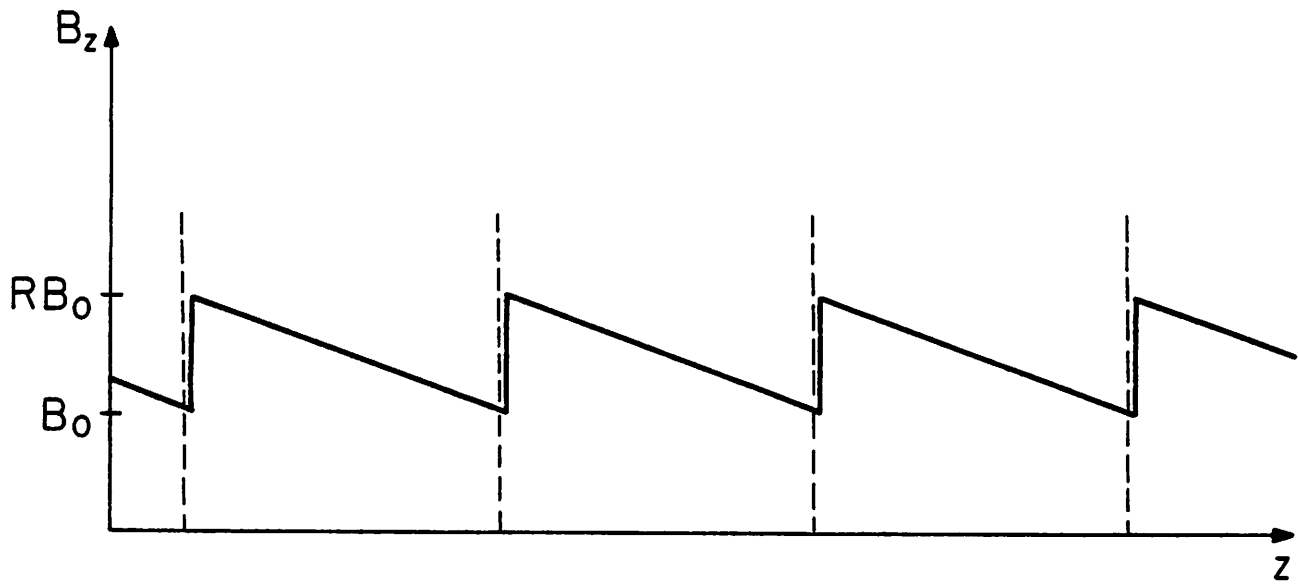


Fig. 1

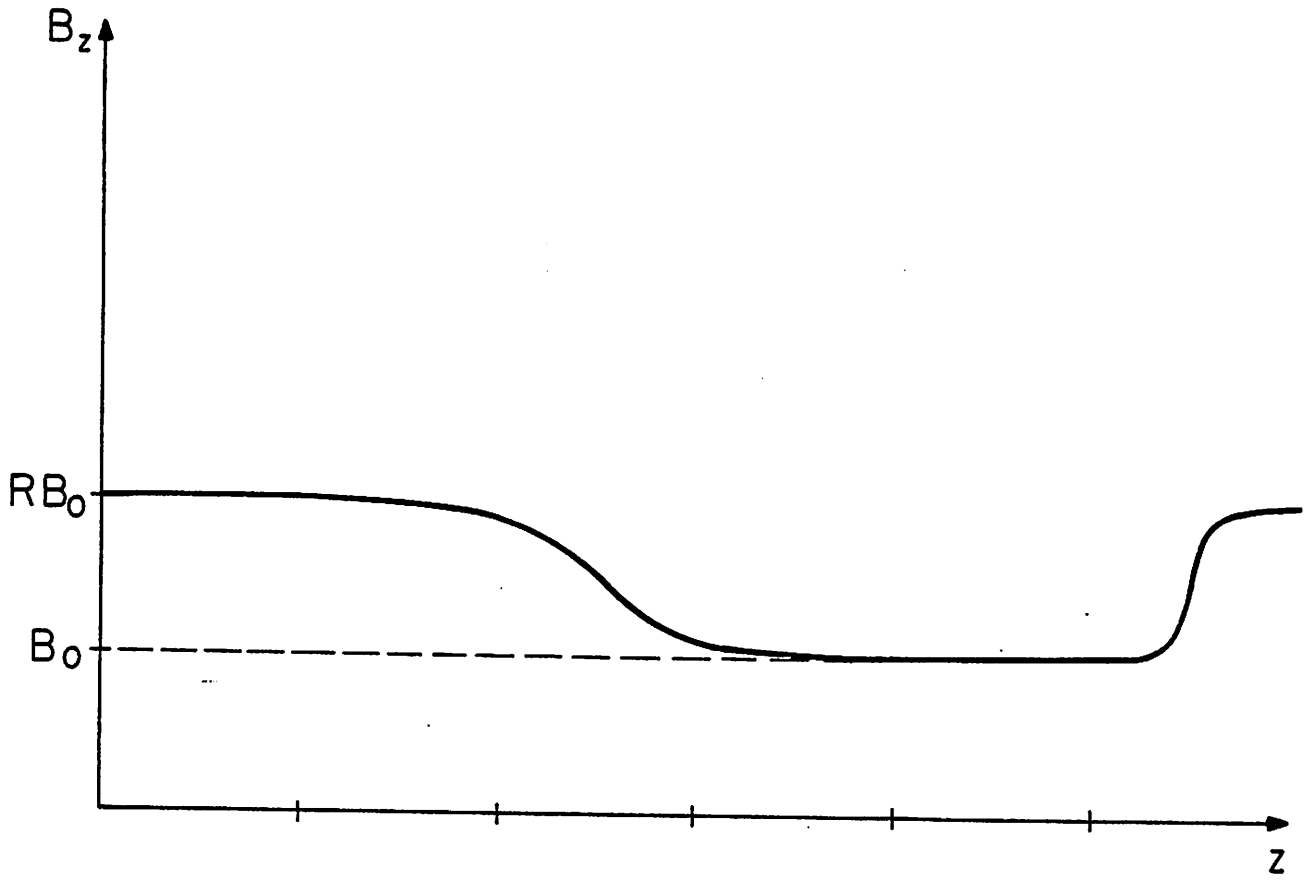


Fig. 2

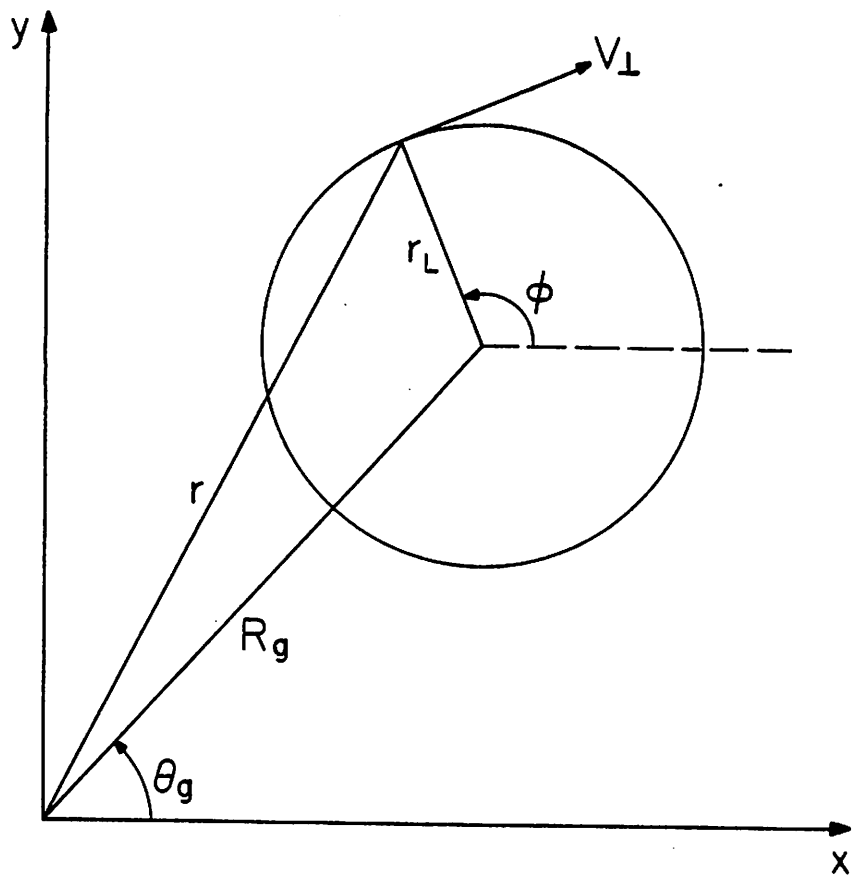


Fig. 3

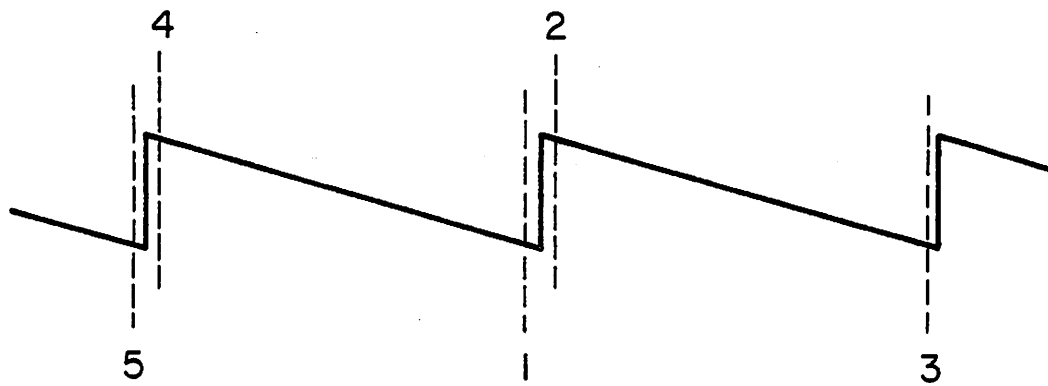


Fig. 4

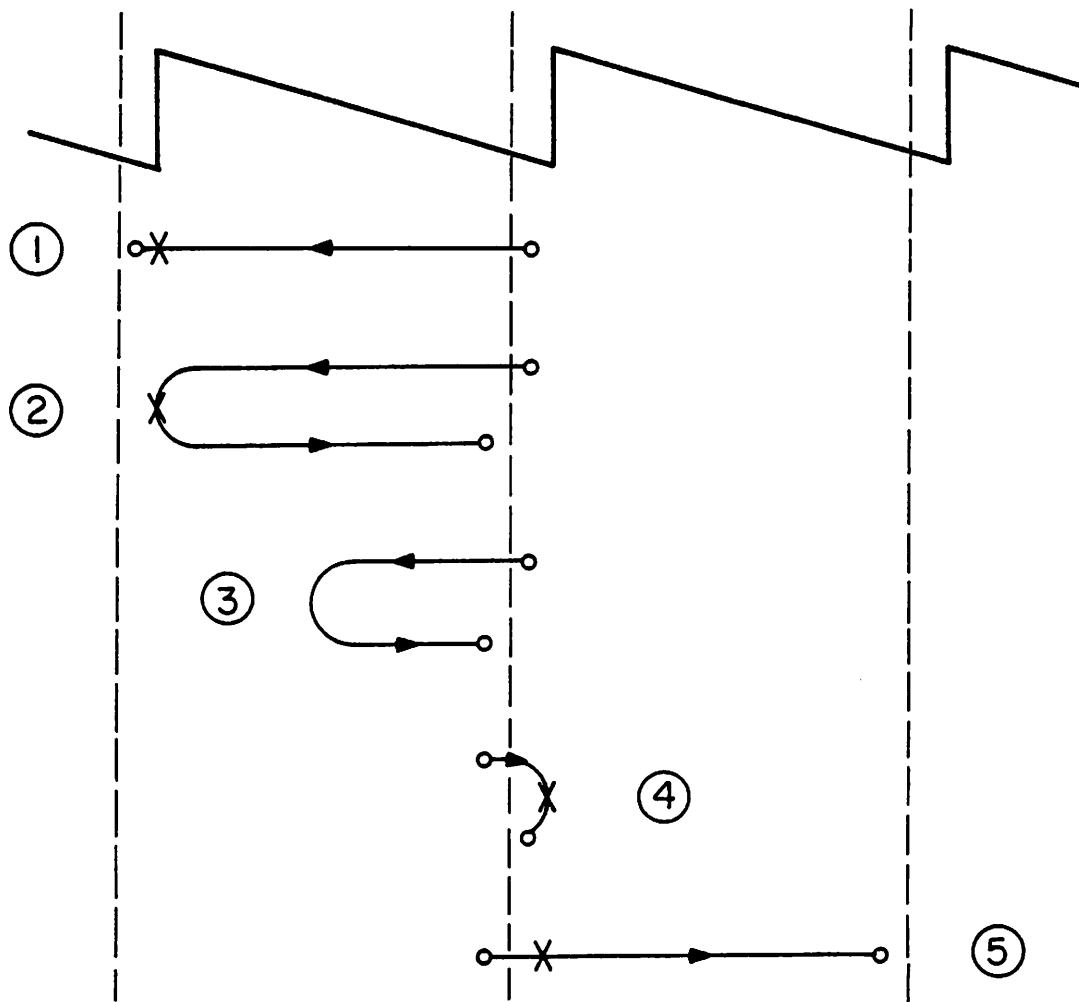


Fig. 5

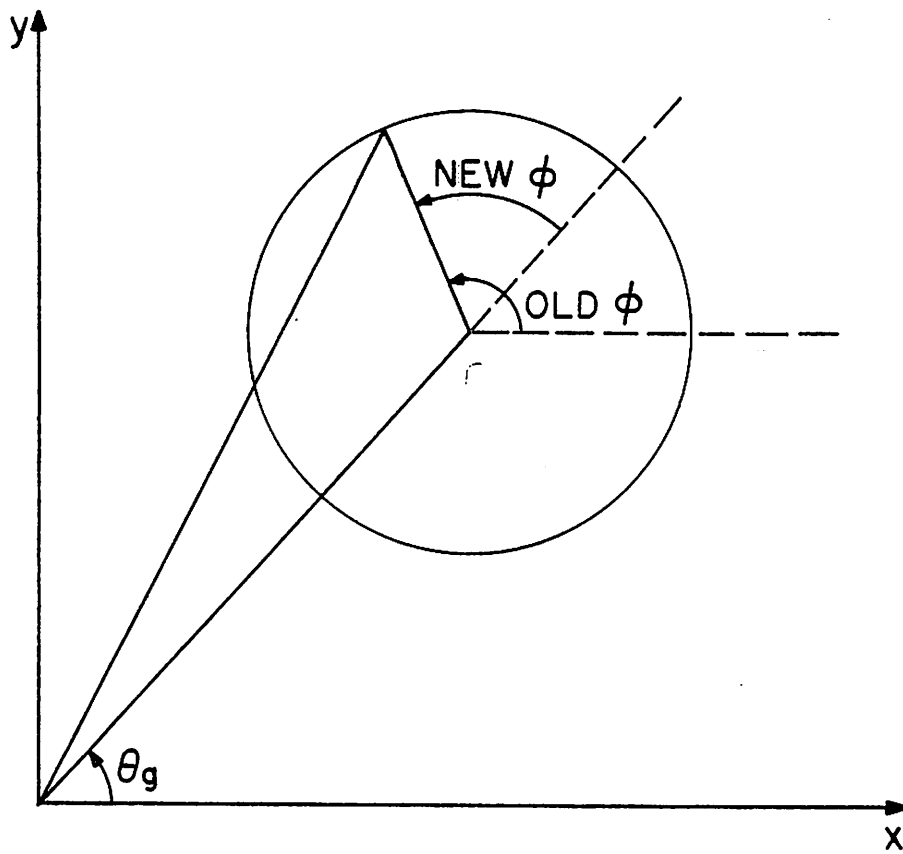
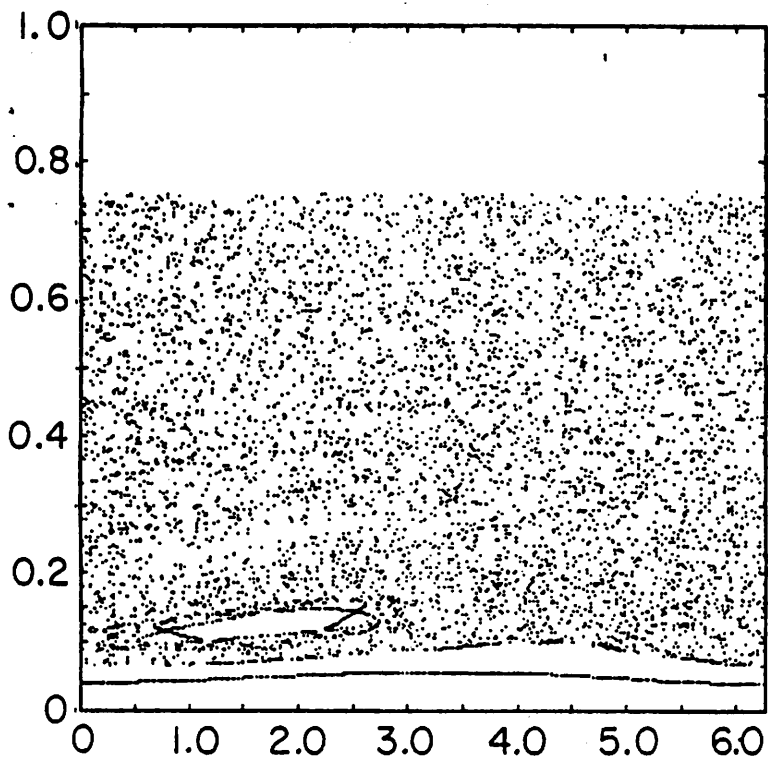
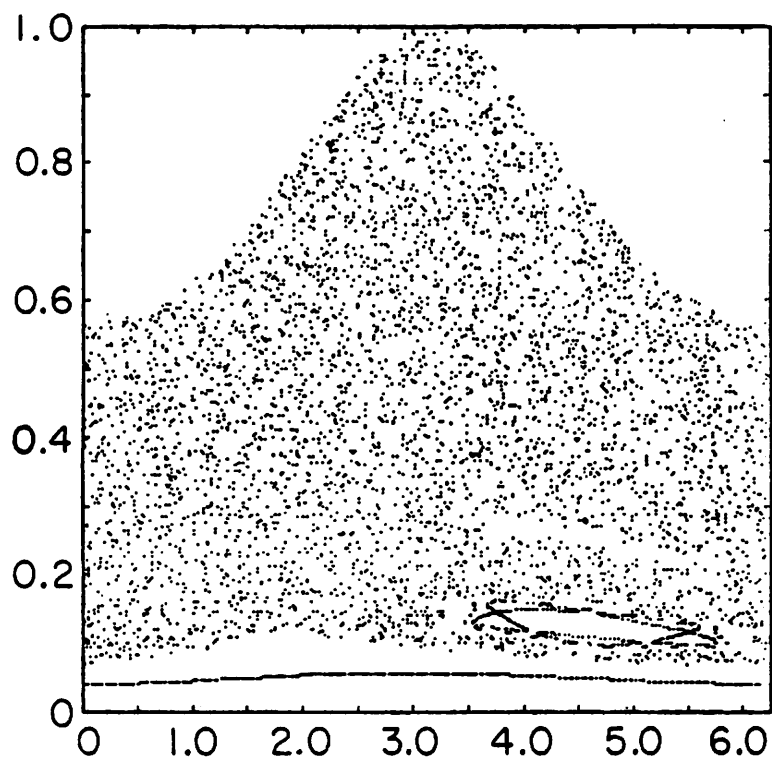


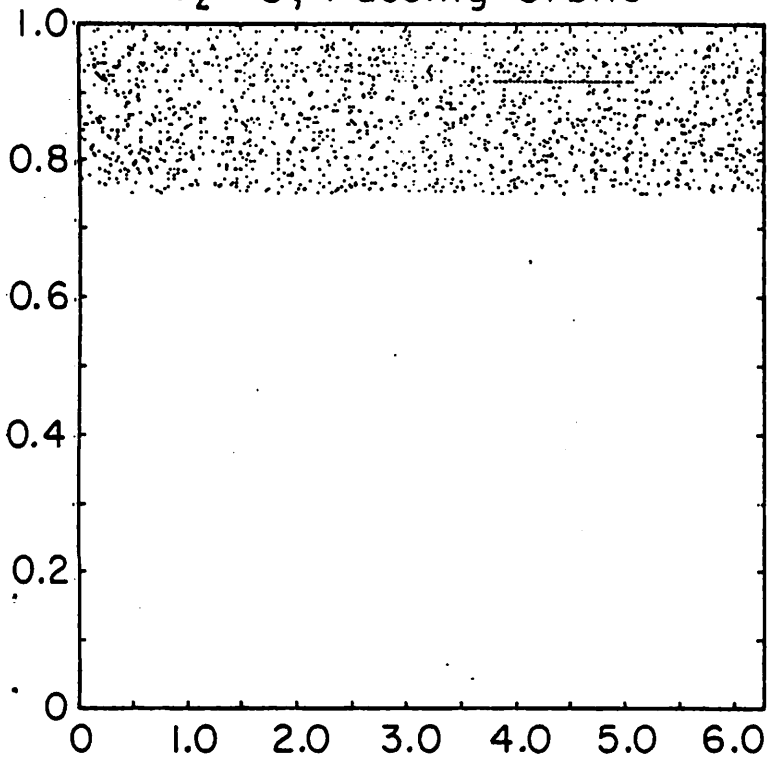
Fig. 6



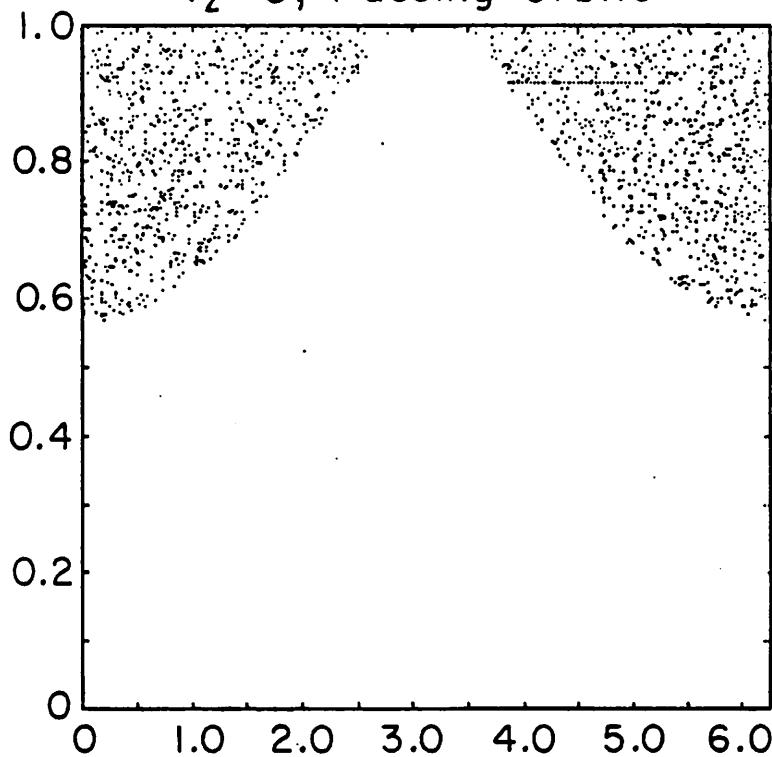
$V_z < 0$, Passing Orbits



$V_z > 0$, Passing Orbits



$V_z < 0$, Trapped Orbits



$V_z > 0$, Trapped Orbits

Fig. 7

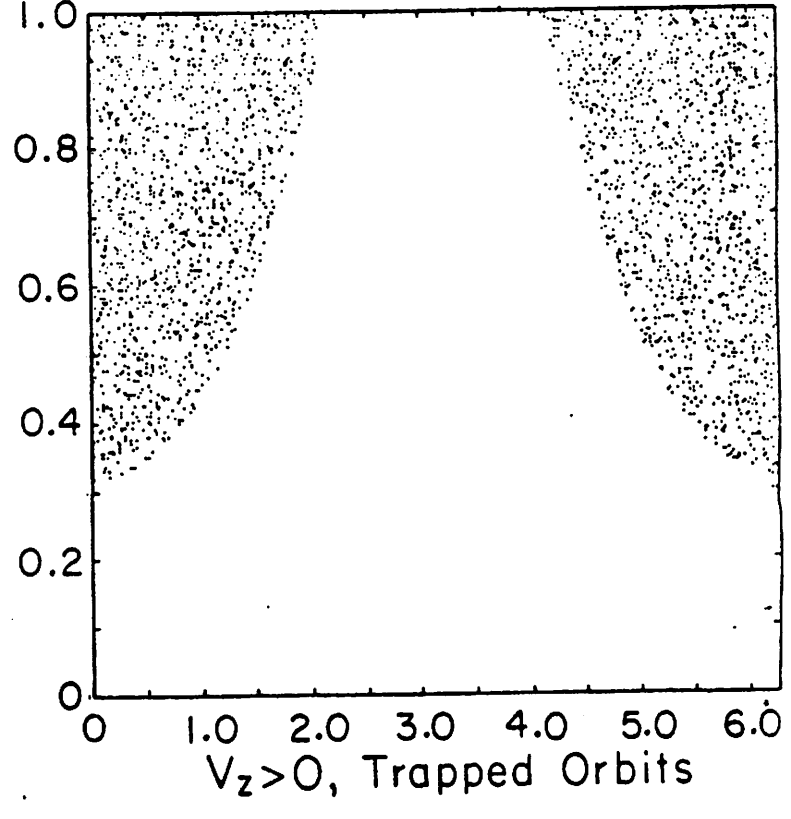
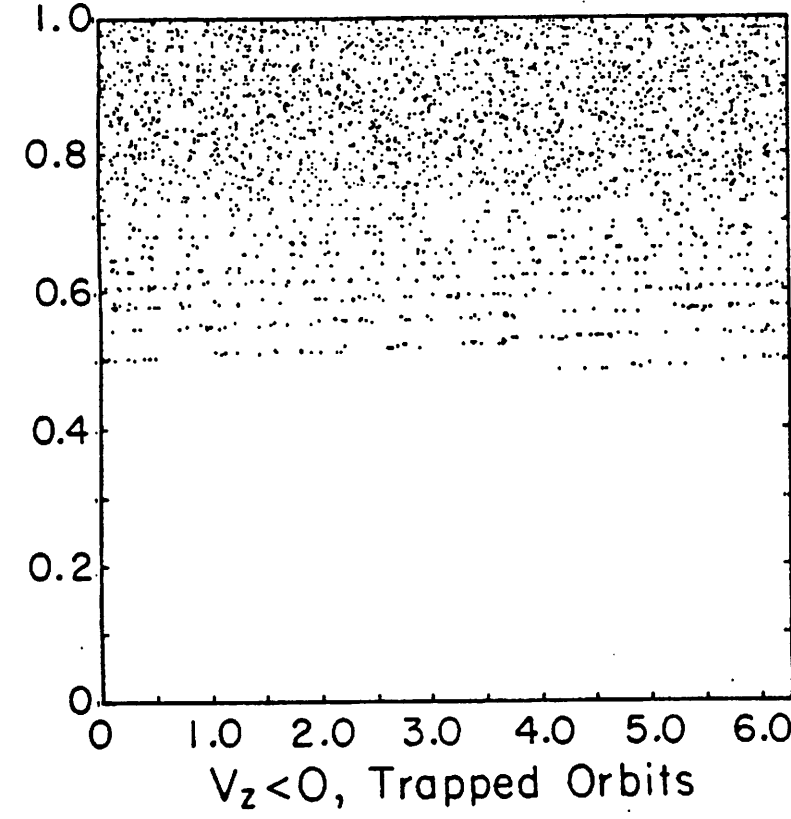
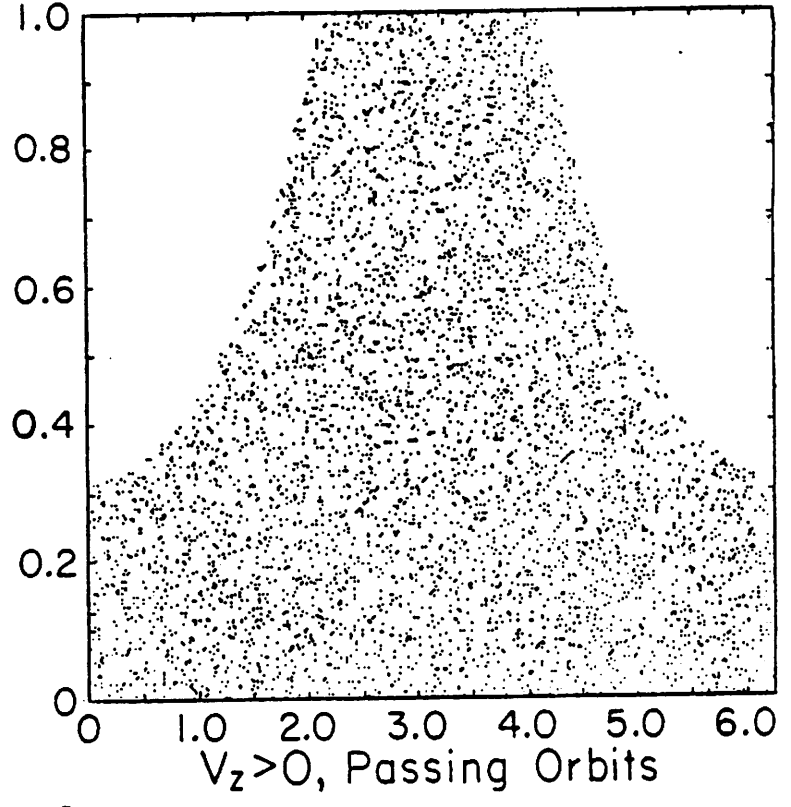
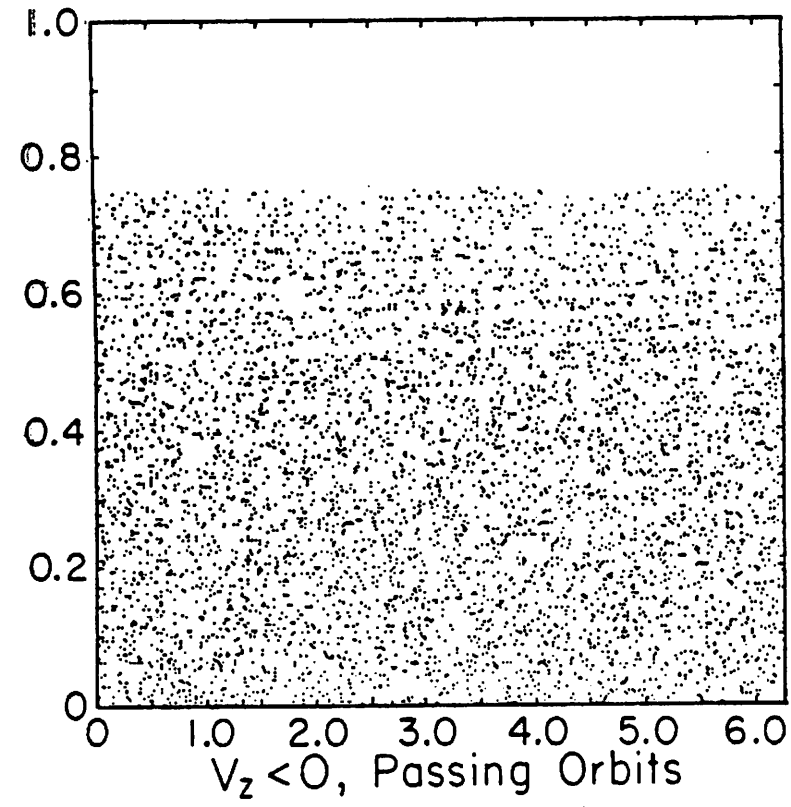


Fig. 8

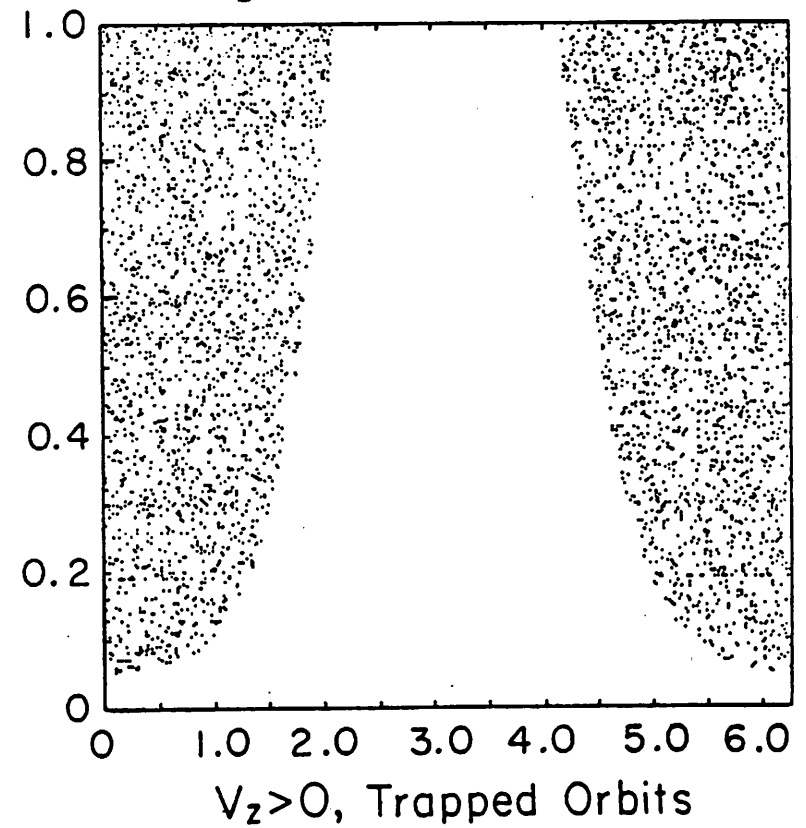
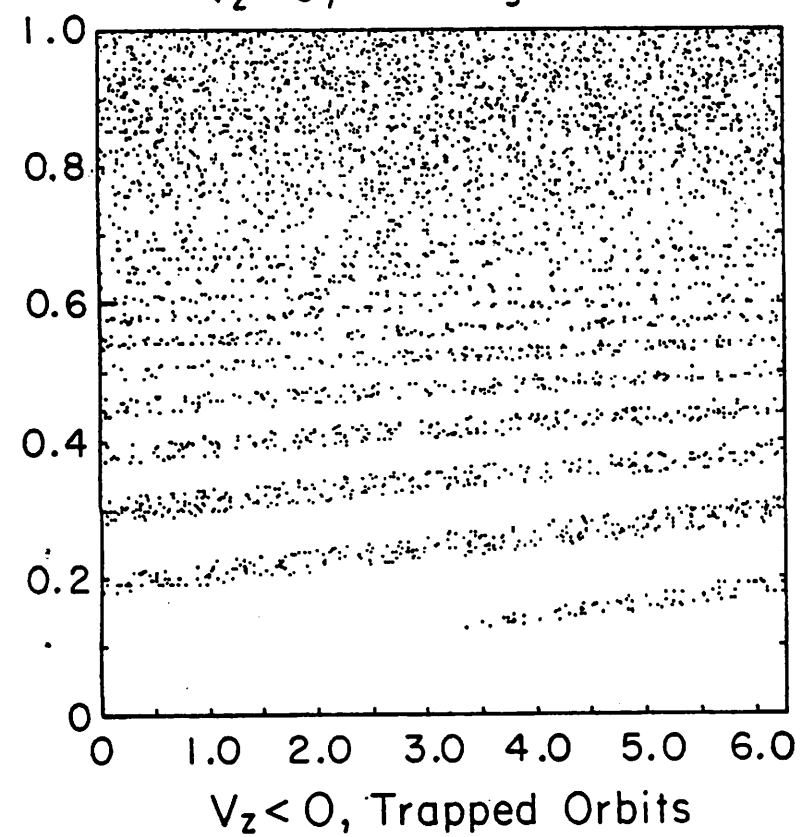
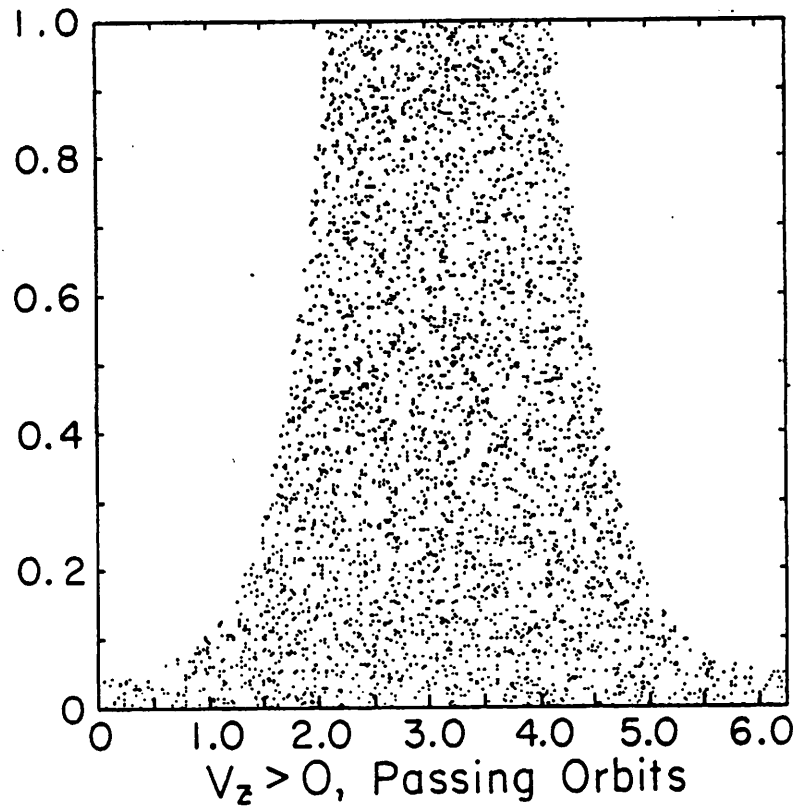
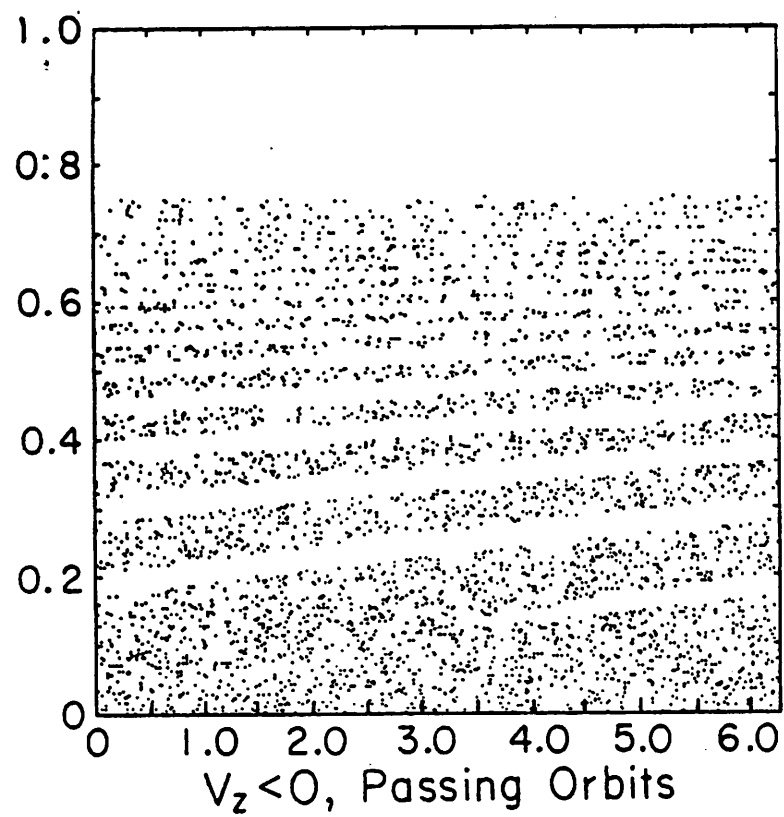


Fig. 9

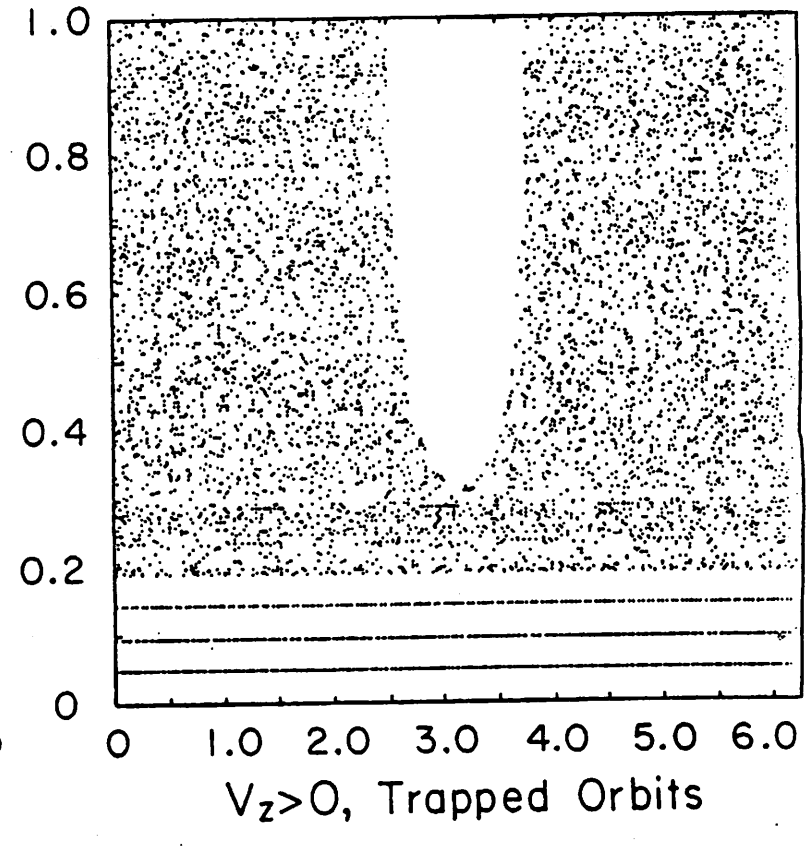
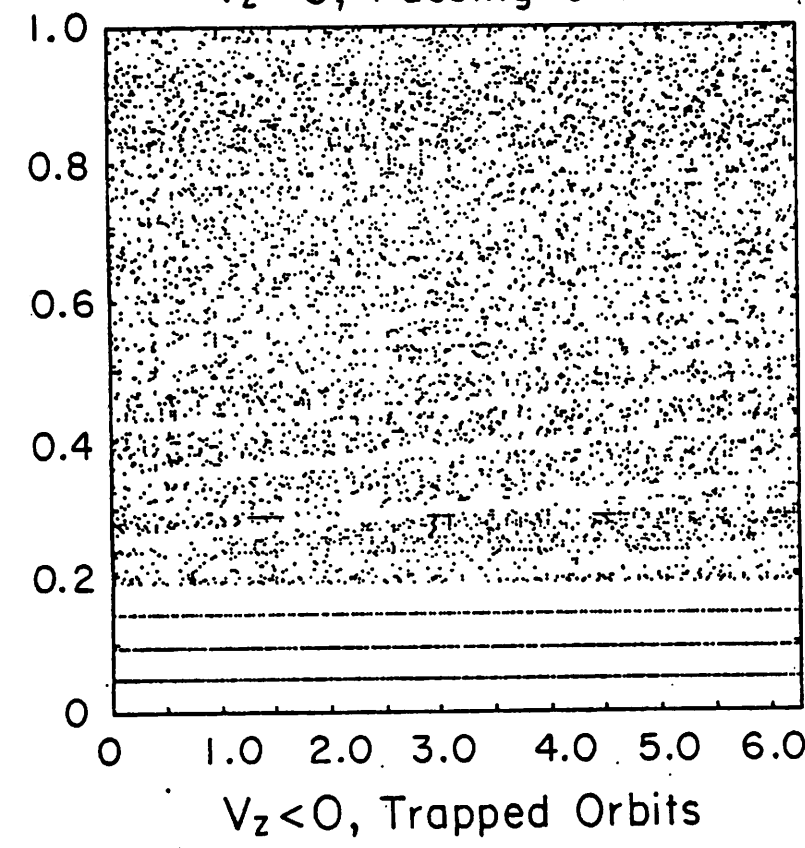
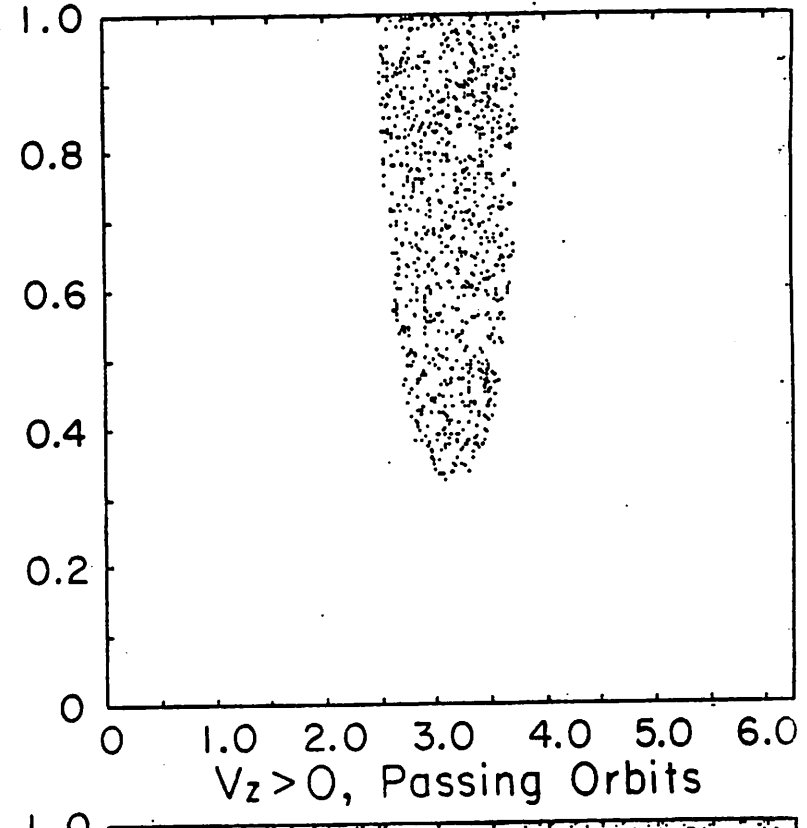
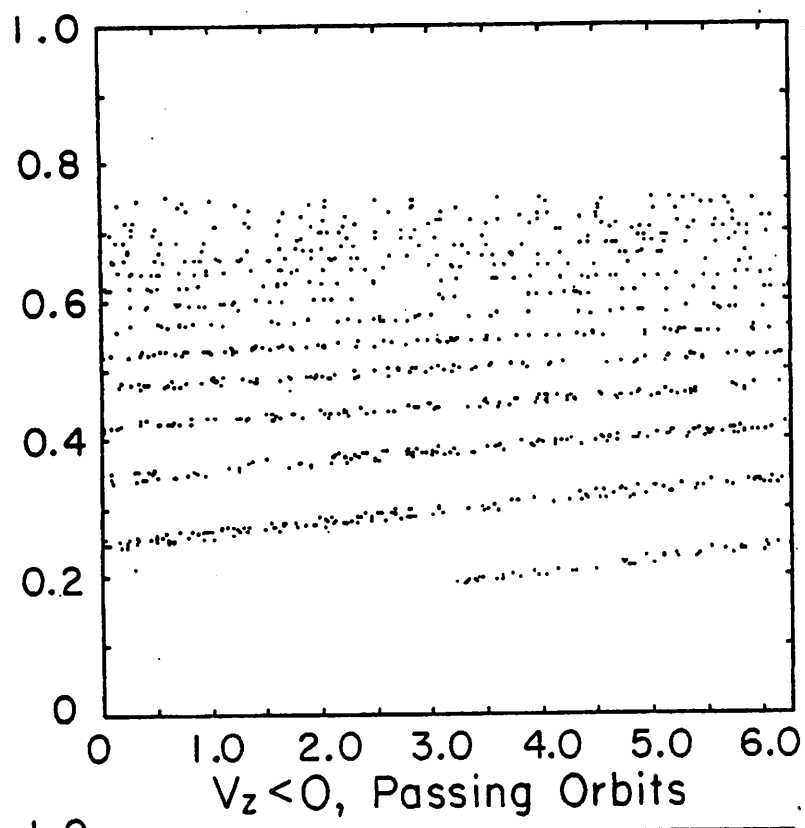
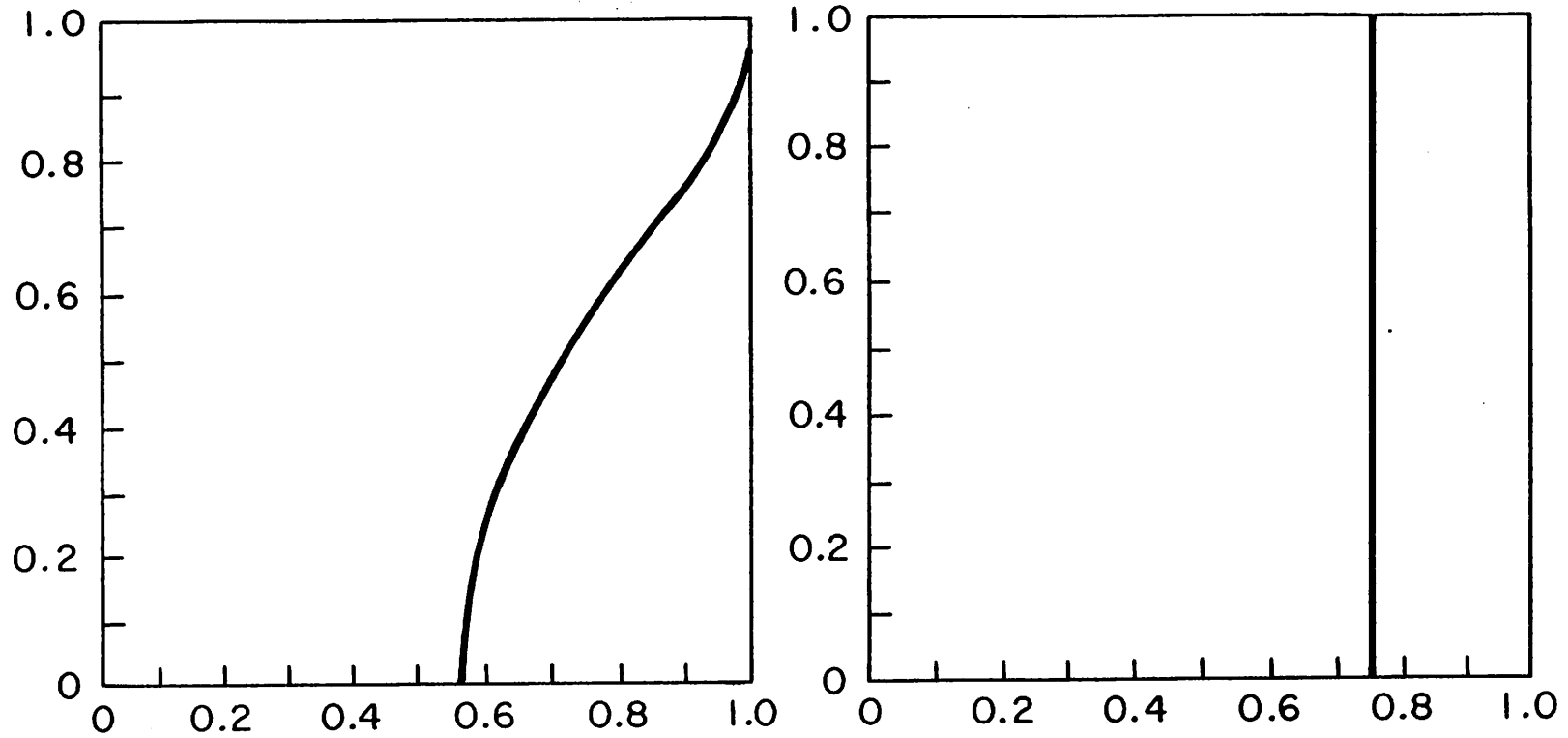


Fig. 10

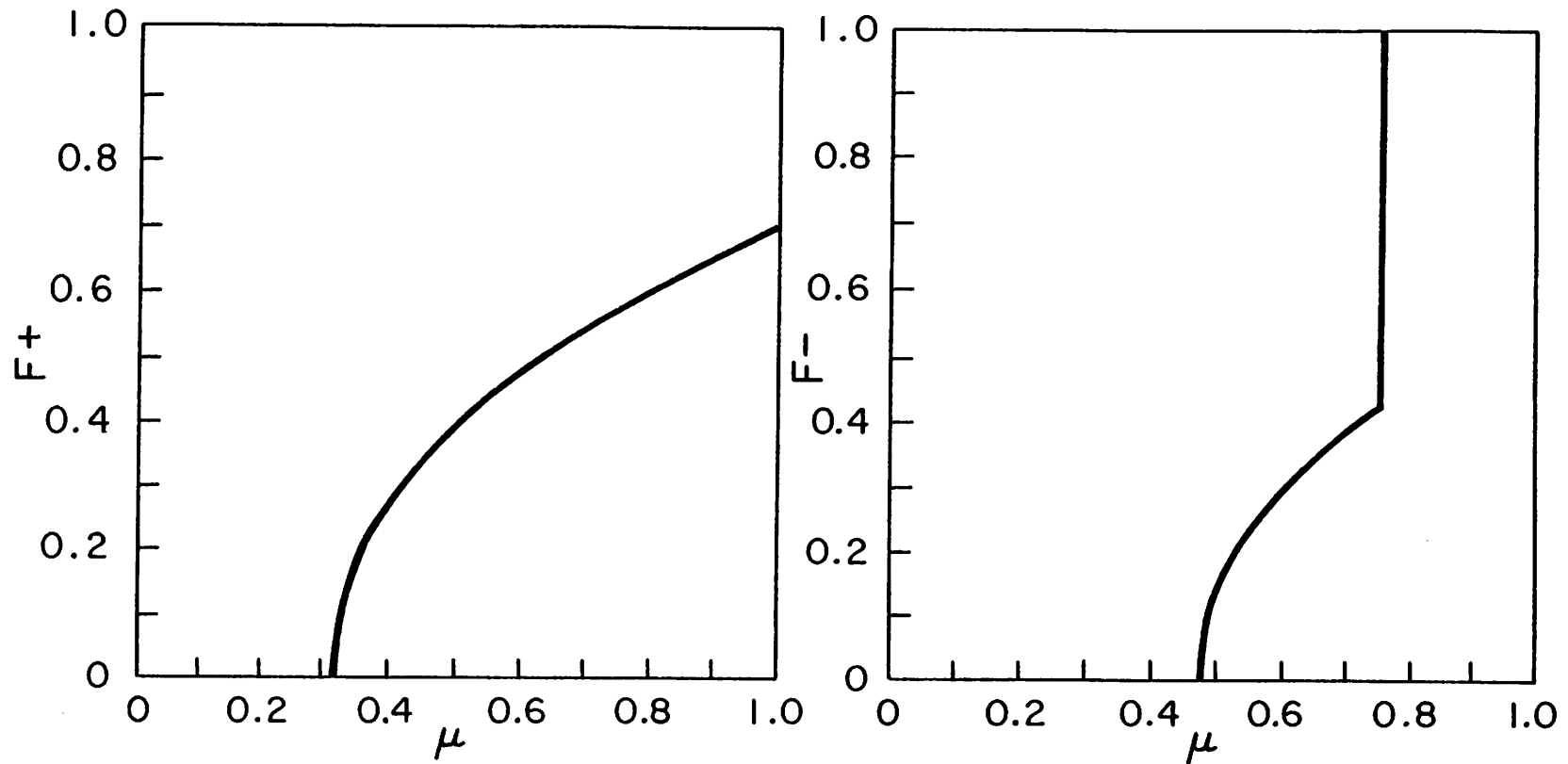


$R=1.33$, $P_{\theta} = 0$; Area under curve is:
 0.248 for $V_z > 0$ & 0.248 for $V_z < 0$

For an isotropic distribution with random gyrophase the total trapping probability is:

0.449 for $V_z > 0$ & 0.488 for $V_z < 0$

Fig. 11

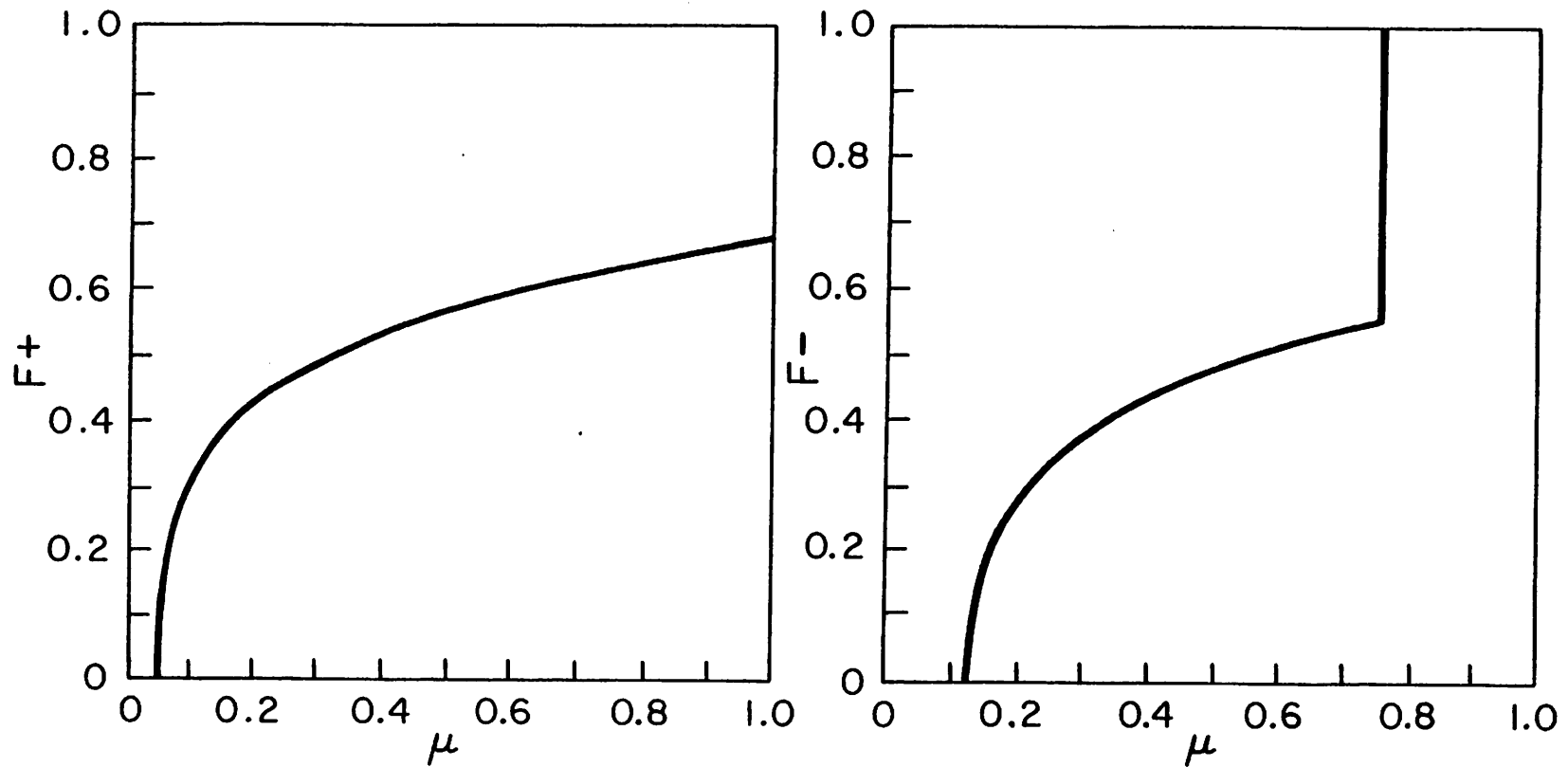


$R = 1.33$, $P_{\theta} = 2.00$; Area under curve is:
 0.327 for $V_z > 0$ & 0.327 for $V_z < 0$

For an isotropic distribution with random gyrophase the total trapping probability is:

0.453 for $V_z > 0$ & 0.555 for $V_z < 0$

Fig. 12



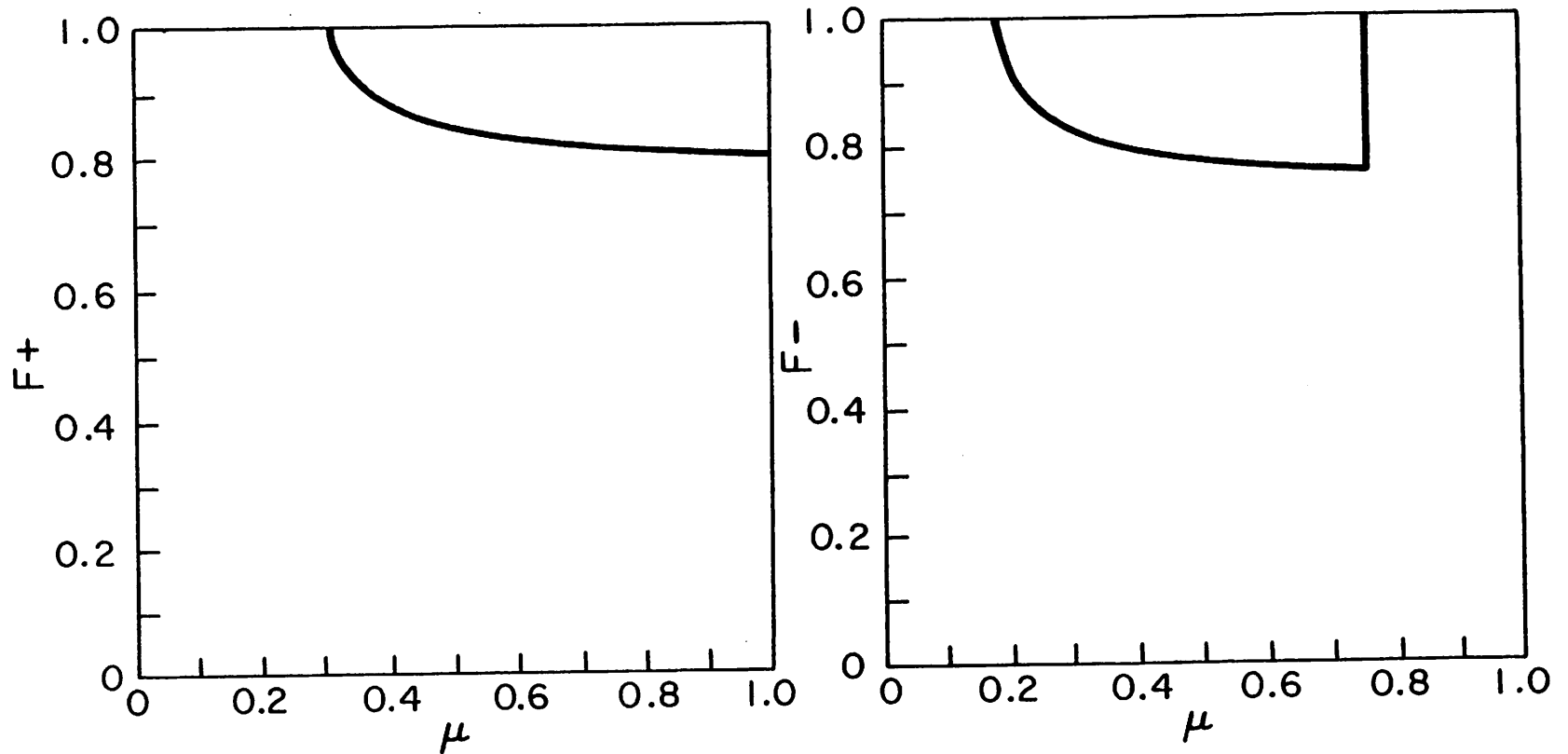
$R=1.33$, $P_{\theta}=10.0$; Area under curve is:

0.511 for $V_z > 0$ & 0.511 for $V_z < 0$

For an isotropic distribution with random gyrophase the total trapping probability is:

0.568 for $V_z > 0$ & 0.680 for $V_z < 0$

Fig. 13



$R=1.33$, $P_{\theta} = 50.0$, Area under curve is:
 0.886 for $V_z > 0$ & 0.886 for $V_z < 0$

For an isotropic distribution with random gyrophase the total trapping probability is:

0.842 for $V_z > 0$ & 0.907 for $V_z < 0$

Fig. 14

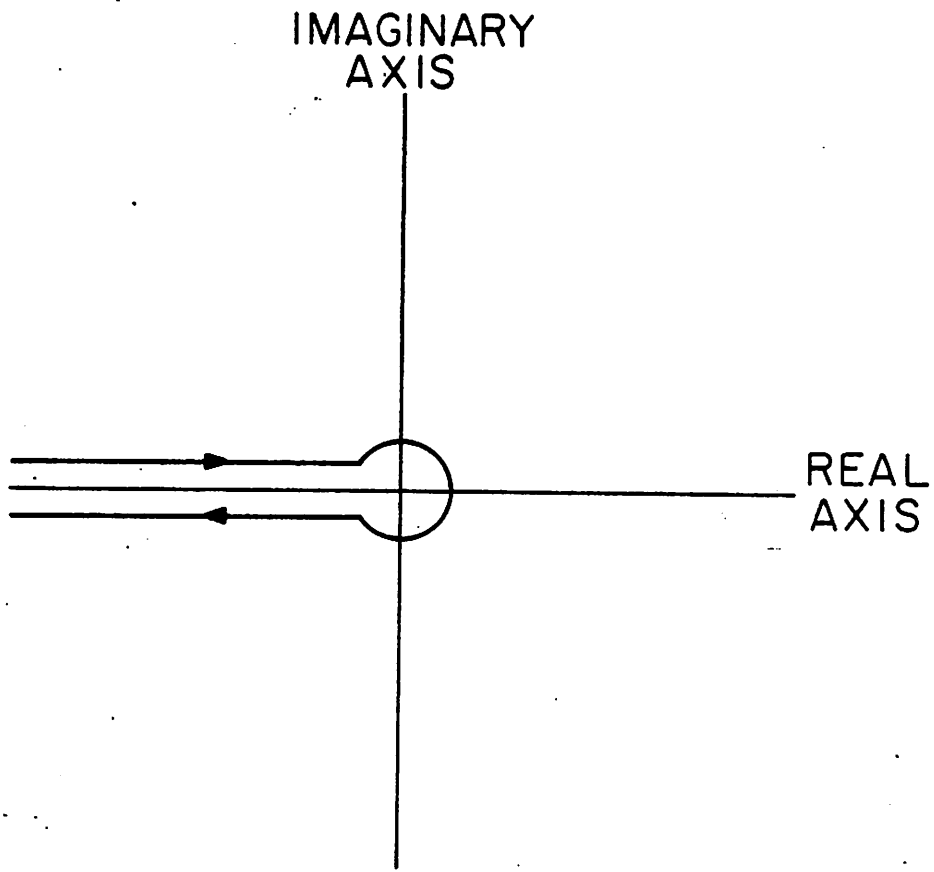


Fig. 15